Int. J. Heat Mass Transfer. Vol. 25, No. 4, pp. 563–573, 1982
Printed in Great Britain

0017-9310/82/040563-11 $03.00/0

AN ANALYSIS OF THE HEAT AND SOLUTE TRANSPORT DURING SOLIDIFICATION OF AN AQUEOUS BINARY SOLUTION—II. DENDRITE TIP REGION

MICHAEL G. O'CALLAGHAN, ERNEST G. CRAVALHO
Massachusetts Institute of Technology, Cambridge, Mass.
and
CHARLES E. HUGGINS
Blood Bank and Transfusion Service, Massachusetts General Hospital, Boston, MA 02114, U.S.A.

(*Received* 29 *October* 1979 *and in revised form* 2 *October* 1981)

Abstract—An analysis of energy and mass transport near the tips of steadily advancing dendrites has been developed. Transport equations have been derived and have been solved using the method of variable transformation to a 1-dim. system. Geometric and thermodynamic matching criteria were employed to ensure that the tip region transport fields were compatible with those obtained previously in the basal plane region.

The overall results indicate that the higher the free field temperature the shorter and more blunt are the dendrites. Similarly increasing the free-field concentration at constant free-field superheat drastically reduces the dendrite length. Dendrite length was also found to be inversely proportional to the rate of freezing.

NOMENCLATURE

a, spheroidal foci coordinate [m];
a', constant in freezing point equation [K];
A_1, A_2, constants in equation (A1);
b', linear coefficient in freezing point equation [K-m^3/mol];
c', quadratic coefficient in freezing point equation [K-m^6/mol^2];
C, concentration [mol/m^3];
$\mathscr{C}$, specific heat [N-m/kg-K];
d', cubic coefficient in freezing point equation [K-m^9/mol^3];
D, diffusion coefficient of solute in solvent [m^2/s];
f, fraction of volume occupied by solid or liquid;
f_s^*, value of f_s at the point of changeover;
$\mathscr{f}$, function defined by equations (23) and (24);
g, function defined by equations (21) and (22);
H, heat flux [W/m^2];
H^*, basal heat flux component due to latent heat of fusion [W/m^2];
k, thermal conductivity [W/m-K];
K, constant of integration;
L, latent heat of fusion [N-m/kg];
L_D, dendrite spacing [m];
L^*, characteristic dendrite length [m];
m', liquidus slope [K-m^3/g-mol];
m, mass flux [g-mol/m^2-s];
P, temperature or concentration;
Pec, Peclet Number $\equiv Ra/\alpha$, Ra/D;
$\dot{q}$, energy flux [N-m/m^2-s];
r, radial coordinate [m];
R, rate of freezing [m/s];
t, time [s];
T, temperature [K];
x, spatial coordinate [m];
x', moving spatial coordinate [m];
$\tilde{Z}$, axial coordinate measured from the spheroidal origin [m];
$\mathscr{Z}$, $= Z - \delta$, displaced axial coordinate [m];
$\tilde{Z}^*$, $= \mathscr{Z}/L^*$, non-dimensional axial coordinate.

Greek symbols

α, thermal diffusivity [m^2/s];
β, constant in paraboloidal equation [m^2];
γ, linear coefficient in paraboloidal equation [m];
δ, spheroidal coordinate displacement [m];
ε, quadratic coefficient in paraboloidal equation;
η, axial spheroidal coordinate;
θ, meridonal spheroidal coordinate;
ρ, density [g/m^3].

Subscripts and superscripts

c, concentration;

change, condition at changeover between basal and tip regions;
eut, eutectic;
f, frontal;
I, interface condition;
ℓ, liquid region;
o, initial condition or oblate coordinates;
p, prolate coordinates;
s, solid region;
sol, solidification;
tip, tip condition;
∞, free-field condition.

INTRODUCTION

IN THE accompanying paper [1], a simple "two-zone" model of energy and mass transport during dendritic solidification was developed. To apply this model, coupled equations describing the temperature and concentration fields are solved for two distinct domains: one near the dendritic basal plane and the other near the dendrite tips. The temperature and concentration profiles from each region are then "matched" using geometric and thermal criteria to insure compatibility and to satisfy the overall boundary conditions.

The object of the present paper is to perform an analysis in the dendrite tip region that is parallel to that done previously in the basal region; that is, to derive energy and mass transport equations and solve for the temperature, concentration and dendrite shape profiles. The simplifying technique used in the dendrite tip region is that of transformation to the oblate–prolate spheroidal coordinate system, in which the iso-potential loci are 1-dim. Solution of the transformed equations yields families of profiles as a function of the boundary conditions.

The present work includes, in addition, a development of the "matching" criteria, which provides a rationale for choosing the specific temperature and concentration profile in each region. The criteria include temperature and heat flux continuity at the point of changeover between the two regions, as well as matching of the dendrite cross-sectional area and surface curvature.

Spheroidal coordinate geometry

A plausible assumption about the shape of the dendrite tips is that their cross-sectional area is parabolic in form:

$$r^2 = \beta + \gamma\tilde{Z} + \varepsilon\tilde{Z}^2 \tag{1}$$

where β, γ and ε are constants, r is the dendrite radius and $\tilde{Z}$ is the axial coordinate, fixed with respect to the dendrite surface. From surface energy considerations, it is known that the tips must be convex out, which places restrictions on possible values of the coefficients β, γ, and ε. The most general mathematical expression of the quadratic form within the convex-out restriction is in the oblate–prolate spheroidal coordinate systems. These systems are shown schematically in Fig. 1 and are mathematically related to the circular cylinder system by

$$\left.\begin{aligned} r &= a\cosh\eta\,\sin\theta \\ \tilde{Z} &= a\sinh\eta\,\cos\theta \end{aligned}\right\}\ \text{oblate}$$

and (2)

$$\left.\begin{aligned} r &= a\sinh\eta\,\sin\theta \\ \tilde{Z} &= a\cosh\eta\,\cos\theta \end{aligned}\right\}\ \text{prolate.}$$

In these equations, a is the distance from the cylindrical origin to the ellipsoidal focus (see Fig. 1). The spheroidal coordinate systems are axially symmetric ellipsoidal systems generated by rotating an orthogonal family of confocal ellipses and hyperbolas about the major (prolate) or minor (oblate) axes of the ellipses.

The surfaces η = constant describe ellipsoids which are identical in form to those described by equation (1) and may be used to express the shape of the dendrite tips and the iso-potential loci. The axial coordinate η ranges from zero to infinity depending upon the degree of "pointedness" of the dendrite tip in either the oblate or prolate case. Oblate spheroids range from flattened discs at $\eta = 0$ to spherical as η approaches infinity and prolate spheroids vary from spherical as η approaches infinity to infinitely pointed as η vanishes. Thus dendrite tips described by the surfaces η = constant may assume any degree of "pointedness", within the convex-out restriction. Dendrite tip configurations for various values of η_{tip} are illustrated in Table 1.

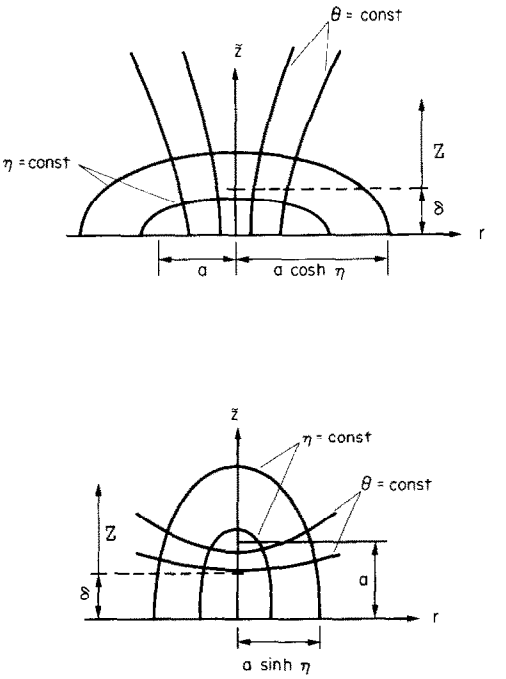

FIG. 1. Schematic representation of the oblate (upper figure) and prolate spheroidal coordinate systems.

Table 1. Dendrite tip configurations and their associated geometric parameters

	η_{tip}	Aspect Ratio	Illustration
OBLATE	0.0	0.0	
	0.5	0.462	
	1.5	0.905	
	3.0	0.995	
PROLATE	3.0	1.01	
	1.5	1.11	
	0.5	2.16	
	0.1	10.0	

To describe the dendrite surface in the form of equation (1), we transform to the $\mathscr{Z}$ coordinate system given by

$$\tilde{Z} = \mathscr{Z} + \delta \tag{4}$$

where $\tilde{Z}$ is measured from the origin of the spheroidal system, $\mathscr{Z}$ is measured from the displaced origin and δ is the origin displacement (see Fig. 1). Using this transformation and eliminating the θ dependence in equations (2) and (3), we obtain

$$r = a\cosh\eta_{tip}\sqrt{1 - \left(\frac{\mathscr{Z} + \delta}{a\sinh\eta_{tip}}\right)^2} \tag{5}$$

(oblate)

and

$$r = a\sinh\eta_{tip}\sqrt{1 - \left(\frac{\mathscr{Z} + \delta}{a\cosh\eta_{tip}}\right)^2} \tag{6}$$

(prolate)

where η_{tip} is the spheroidal coordinate describing the dendrite surface. The maximum apparent radius of the dendrite tip when viewed along the $-\mathscr{Z}$ axis (the dendrite frontal radius) may be obtained from equations (5) and (6).

Setting $\mathscr{Z}$ to $-\delta$, we obtain

$$r_f = a\cosh\eta_{tip} \quad \text{(oblate)} \tag{7}$$

and

$$r_f = a\sinh\eta_{tip} \quad \text{(prolate)}. \tag{8}$$

Finally, equations (5) and (6) may be non-dimensionalized using the transformations:

$$\tilde{Z}^* = \mathscr{Z}/L^* \tag{9}$$

and

$$f_s = \frac{\pi r^2}{\pi L_D^2} \tag{10}$$

to obtain

$$f_s = \left(\frac{a}{L_D}\right)^2\cosh^2\eta_{tip} - \tilde{Z}^{*2}\left(\frac{L^*}{L_D}\right)^2\coth^2\eta_{tip} - 2\tilde{Z}^*\left(\frac{\delta L^*}{L_D^2}\right)\coth^2\eta_{tip} - \left(\frac{\delta}{L_D}\right)^2\coth^2\eta_{tip}$$

(oblate) (11)

and

$$f_s = \left(\frac{a}{L_D}\right)^2\sinh^2\eta_{tip} - \tilde{Z}^{*2}\left(\frac{L^*}{L_D}\right)^2\tanh^2\eta_{tip} - 2\tilde{Z}^*\frac{\delta L^*}{L_D^2}\tanh^2\eta_{tip} - \left(\frac{\delta}{L_D}\right)^2\tanh^2\eta_{tip}$$

(prolate) (12)

where

$$L^* = \frac{(k_s - k_\ell)f_s^\circ + k_\ell}{R[(\rho_s\mathscr{C}_s - \rho_\ell\mathscr{C}_\ell)f_s^\circ + \rho_\ell\mathscr{C}_\ell]} \tag{13}$$

and L_D is the dendrite spacing (see Appendix). The parameter f_s represents the fraction of the cross-sectional area at any position that is occupied by ice.

ENERGY AND MASS TRANSPORT NEAR DENDRITE TIPS

Transport equations

Ivantsov [2] analyzed heat and mass transport in the vicinity of dendrite tips described by equation (1) and indicated that the isotherms and isoconcentrates are mathematically identical in form to the dendrite tip equation. This implies that the temperature and concentration fields are 1-dim in the axial coordinate, η.

The 1-dim. ordinary differential equations describing the energy and solute transport have been derived by [6]:

$$\frac{\partial^2 T_j}{\partial \eta^2} + [Pec_j \cosh \eta + \tanh \eta]\frac{\partial T_j}{\partial \eta} = 0, \quad (14)$$

$$\frac{\partial^2 C}{\partial \eta^2} + [Pec_c \cosh \eta + \tanh \eta]\frac{\partial C}{\partial \eta} = 0 \quad (15)$$

for the oblate spheroidal geometry, and

$$\frac{\partial^2 T_j}{\partial \eta^2} + [Pec_j \sinh \eta + \coth \eta]\frac{\partial T_j}{\partial \eta} = 0 \quad (16)$$

$$\frac{\partial^2 C}{\partial \eta^2} + [Pec_c \sinh \eta + \coth \eta]\frac{\partial C}{\partial \eta} = 0 \quad (17)$$

for the prolate spheroidal case, where

$$Pec_c = aR/D \quad (18)$$

and

$$Pec_j = aR/\alpha_j, \quad j = s, \ell. \quad (19)$$

Comparison of equations (14)–(17) shows that the temperature and concentration fields will be geometrically similar in form but will in general have different parametric distortion. The solution to equations (14)–(17) is given by

$$P_i(\eta) - P_\infty = K_j^i g_j(Pec_i, \eta), \quad (20)$$

$$i = s, \ell, c; \quad j = \text{oblate, prolate}$$

where $P_s = T_s$, $P_\ell = T_\ell$ and $P_c = C$, and the K_j^i are constants of integration. The functions g_j are given by

$$g_{\text{oblate}} = \int_\eta^\infty \mathcal{I}_{\text{oblate}}\, d\eta, \quad (21)$$

$$g_{\text{prolate}} = \int_\eta^\infty \mathcal{I}_{\text{prolate}}\, d\eta \quad (22)$$

where

$$\mathcal{I}_{\text{oblate}} = \frac{\exp(-Pec_i \sinh \eta)}{\cosh \eta}, \quad (23)$$

and

$$\mathcal{I}_{\text{prolate}} = \frac{\exp(-Pec_i \cosh \eta)}{\sinh \eta}. \quad (24)$$

Boundary conditions

The boundary conditions for the temperature and concentration fields are summarized in Table 2. In the freezing of most aqueous solutions, solute molecules are excluded completely from the advancing ice crystal. This condition is expressed mathematically by setting the solute particle velocity to zero in the dendrite–surface–fixed coordinate system. By neglecting the volume change associated with freezing†, we obtain

$$\frac{\partial C}{\partial \eta}(\eta_{tip}) + Pec_c \sinh(\eta_{tip})\, C(\eta_{tip}) = 0 \quad (25)$$

and

$$\frac{\partial C}{\partial \eta}(\eta_{tip}) + Pec_c \cosh(\eta_{tip})\, C(\eta_{tip}) = 0 \quad (26)$$

for the prolate and oblate cases respectively. The conditions are applied at $\eta = \eta_{tip}$ which represents the front surface of the advancing dendrite.

The temperature profiles described by equation (20) must "match" at the dendrite surface. Then

$$T_s(\eta_{tip}) = T_\ell(\eta_{tip}) = T_I. \quad (27)$$

If we assume that the solid phase and the liquid solution just adjacent to it are essentially in local thermodynamic equilibrium, the interface concentration will determine the interface temperature from the locus of two-phase equilibrium states. This locus may be approximated by a power series of the form

$$T_I = a' + b' C(\eta_{tip}) + c' C^2(\eta_{tip}) + d' C^3(\eta_{tip}). \quad (28)$$

The rate of liberation of the latent heat of fusion is controlled by the rate of advance of the dendrite. Conservation of energy applied to a control volume centered on the dendrite surface gives

$$k_s \frac{dT_s}{d\eta}(\eta_{tip}) - k_\ell \frac{dT_\ell}{d\eta}(\eta_{tip}) = aR\rho_s L \sinh(\eta_{tip}) \quad (29)$$

for the prolate coordinates; and

$$k_s \frac{dT_s}{d\eta}(\eta_{tip}) - k_\ell \frac{dT_\ell}{d\eta}(\eta_{tip}) = aR\rho_s L \cosh(\eta_{tip}) \quad (30)$$

for the oblate coordinates. The left-hand sides of equations (29) and (30) represent the net heat flux out of the control volume as calculated by the Fourier conduction law, which is equated to the rate of liberation of the latent heat of fusion.

In addition to satisfying conservation of energy and solute, a dendrite stability condition must be imposed at the dendrite tip. Dendrites are formed from the growth of perturbations of a morphologically unstable planar interface. This structural change tends to relieve instability as the system approaches a stable, quasi-steady state. The tip configuration at steady state is that which just eliminates the instability, and is termed *marginally* stable.

The Mullins–Sekerka stability criterion [3] which

†As stated in the preceding paper, this volume change would give rise to a relative motion between the solid and liquid regions. Its effect is considered negligible.

Table 2. Boundary conditions at the dendrite tip

	Prolate	Oblate
Concentration	$\frac{\partial C}{\partial \eta}(\eta_{tip}) + Pec_c \sinh(\eta_{tip}) C(\eta_{tip}) = 0$	$\frac{\partial C}{\partial \eta}(\eta_{tip}) + Pec_c \cosh(\eta_{tip}) C(\eta_{tip}) = 0$
Temperature	$T_s(\eta_{tip}) = T_\ell(\eta_{tip}) = a' + b'C(\eta_{tip}) + c'C(\eta_{tip})^2 + d'C(\eta_{tip})^3$	
	$k_s \frac{dT_s}{d\eta}(\eta_{tip}) - k_\ell \frac{dT_\ell}{d\eta}(\eta_{tip}) = aR\rho_s L \sinh(\eta_{tip})$	$k_s \frac{dT_s}{d\eta}(\eta_{tip}) - k_\ell \frac{dT_\ell}{d\eta}(\eta_{tip}) = aR\rho_s L \cosh(\eta_{tip})$
Marginal stability condition	$\frac{\partial C}{\partial \mathscr{Z}}(\eta_{tip}) \cdot \frac{\partial T_l}{\partial C} - \frac{1}{k_s + k_\ell}\left[k_s \frac{dT_s}{d\mathscr{Z}}(\eta_{tip}) + k_\ell \frac{dT_\ell}{d\mathscr{Z}}(\eta_{tip})\right] \le 0$	

was developed for planar freezing, applies equally well to the present case. The criterion mathematically expresses the condition of stability of a given dendrite configuration and will apply as a coupled boundary condition on the transport fields. The criterion is:

$$\frac{\partial C}{\partial \mathscr{Z}}(\eta_{tip}) \cdot \frac{\partial T_l}{\partial C} - \frac{1}{k_s - k_\ell} \times \left[k_s \frac{dT_s}{d\mathscr{Z}}(\eta_{tip}) + k_\ell \frac{dT_\ell}{d\mathscr{Z}}(\eta_{tip})\right] \le 0 \quad (31)$$

where the terms are expressed by equations (20), (25), (26) and (28). The first term of equation (31) represents the gradient in the liquidus temperature; it is always positive and thus is a destabilizing influence. The second term represents the interface temperature gradient; it is always negative and favors stability. Marginal stability of the interface occurs if the two terms are equal in magnitude. Marginally stable dendrites and the equality of equation (31) is the case considered here.

Equations (25)–(30) may be used in equation (20) to solve for the constants of integration, K_j^i. After rearranging, these constants are given by

$$K_o^c = \frac{C_\infty Pec_c \cosh \eta_{tip}}{\mathscr{I}_o(Pec_c, \eta_{tip}) - Pec_c \cosh \eta_{tip}\, g_o(Pec_c, \eta_{tip})}, \quad (32)$$

$$K_p^c = \frac{C_\infty Pec_c \cosh \eta_{tip}}{\mathscr{I}_p(Pec_c, \eta_{tip}) - Pec_c \sinh \eta_{tip} g_p(Pec_c, \eta_{tip})}, \quad (33)$$

$$K_o^\ell = \frac{T_I - T_\infty}{g_o(Pec_\ell, \eta_{tip})}, \quad (34)$$

$$K_p^\ell = \frac{T_I - T_\infty}{g_p(Pec_\ell, \eta_{tip})}, \quad (35)$$

$$K_p^s = \frac{k_\ell}{k_s} K_p^\ell \frac{\mathscr{I}_p(Pec_\ell, \eta_{tip})}{\mathscr{I}_p(Pec_s, \eta_{tip})} - \frac{R\rho_s L}{k_s} a \sinh \eta_{tip} \quad (36)$$

and

$$K_o^s = \frac{k_\ell}{k_s} K_o^\ell \frac{\mathscr{I}_o(Pec_\ell, \eta_{tip})}{\mathscr{I}_o(Pec_s, \eta_{tip})} - \frac{R\rho_s L}{k_s} a \cosh \eta_{tip} \quad (37)$$

where $T(\eta_{tip})$ is the temperature at the dendrite surface given by equation (28) with $C(\eta_{tip})$ given by equation (25) or (26). By using these constants in equations (20) and (31) and by specifying the dendrite frontal radius and the rate of freezing, the concentration and temperature profiles in the vicinity of the advancing dendrite may be obtained.

Spheroidal coordinate results

The non-dimensional temperature and concentration profiles are plotted in Figs. 2 and 3. These plots represent a comparison of profiles near marginally stable dendrites of a constant frontal radius of 100 μm, in order to illustrate the effect of freezing rate. The frontal radius, given by equations (7) and (8), may be substituted into the definition of Peclet number to yield

$$Pec_c = \frac{R(100\,\mu m)}{D \sinh(\eta_{tip})} \quad \text{(prolate)}, \quad (38)$$

$$Pec_c = \frac{R(100\,\mu m)}{D \cosh(\eta_{tip})} \quad \text{(oblate)}, \quad (39)$$

$$Pec_j = \frac{R(100\,\mu m)}{\alpha_j \sinh(\eta_{tip})} \quad \text{(prolate)} \quad (40)$$

and

$$Pec_j = \frac{R(100\,\mu m)}{\alpha_j \cosh(\eta_{tip})} \quad \text{(oblate)}, \quad j = s, \ell. \quad (41)$$

Thus as the rate of freezing is varied from 10 μm/s to 1000 μm/s, the Peclet numbers must be changed according to equations (38)–(41) to maintain the frontal radius at 100 μm. Physical constants used in the solution are identical to those used in the previous paper [1].

The concentration and temperature profiles are expressed in terms of the "unaccomplished potential change" or the fraction the potential has changed from the interface value to the free-field value. To specify the potential fields completely, the interface concentration must be calculated from equation (20) and the cor-

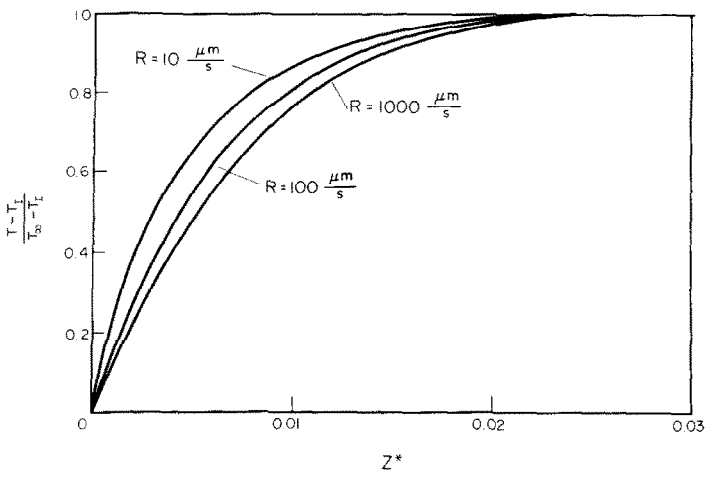

FIG. 2. Non-dimensional temperature profiles in the vicinity of dendrites growing at various rates. Dendrite frontal radius is constant at 100 μm.

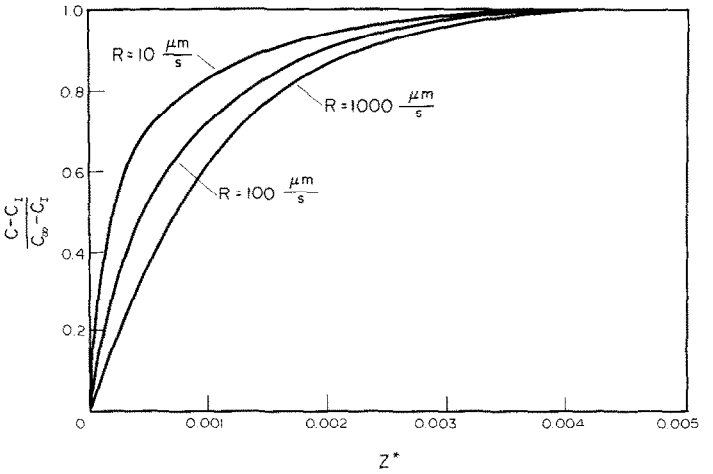

FIG. 3. Non-dimensional concentration profiles in the vicinity of dendrites (r_t = 100 μm) growing at various rates.

responding interface temperature calculated from equation (28). These parameters are plotted in Fig. 4. The three factors that increase the interface concentration (decrease the interface temperature) are increasing the bluntness of the dendrite tip, increasing the rate of freezing and increasing the dendrite frontal radius. Since the tip bluntness is fixed by the requirement of marginal stability and the frontal radius is fixed by definition (100 μm), Fig. 4 illustrates the effect of rate of freezing only.

The temperature and concentration profiles shown in Figs. 2 and 3 are qualitatively similar since they are both solutions to equation (20) with different Peclet numbers and boundary conditions. The variation of both profiles is of the form $\exp(Pec \cdot \exp \eta)$. This functional form causes a drastic change in the potentials near the dendrite surface but a much slower change as the free-field is approached.

BASAL REGION—TIP REGION MATCHING CRITERIA

Limit of basal region

The assumption of planar iso-potential loci places limits on the region of applicability of the basal region solution. The assumption becomes invalid when the dendrite area changes substantially with axial position. It can be shown [4] that the overall solution is very insensitive to the number chosen for the termination value of $df_s/d\bar{Z}^*$, provided that it is greater than 0.2. Therefore, the criterion for terminating the basal region and starting the tip region will be assumed when the magnitude of $df_s/d\bar{Z}^*$ exceeds 0.2.

Geometric compatibility

The basic idea behind the "two-zone" solution scheme is to use the basal region solution to describe the dendrite shape up to a changeover point and then

to determine a spheroidal cap that matches with this dendrite base. Therefore, the values of f_s and $df_s/d\tilde{Z}^*$ predicted by the basal solution must be equal to the values predicted by the tip region solution at the point of changeover. By definition, $\tilde{Z}^* = 0$ at the point of changeover, so using equations (11) and (12) we obtain

$$f_s(\text{changeover}) = \left(\frac{a}{L_D}\right)^2 \cosh^2\eta_{tip} - \left(\frac{\delta}{L_D}\right)^2 \coth^2\eta_{tip} \quad (42)$$

$$\equiv f_s^*,$$

$$\frac{df_s}{d\tilde{Z}^*}(\text{changeover}) = -2\left(\frac{\delta L^*}{L_D^2}\right)\coth^2\eta_{tip} \quad (43)$$

for the oblate case, and

$$f_s(\text{changeover}) = \left(\frac{a}{L_D}\right)^2 \sinh^2\eta_{tip} - \left(\frac{\delta}{L_D}\right)^2 \tanh^2\eta_{tip} \quad (44)$$

$$\equiv f_s^*,$$

$$\frac{df_s}{d\tilde{Z}^*}(\text{changeover}) = -2\left(\frac{\delta L^*}{L_D^2}\right)\tanh^2\eta_{tip} \quad (45)$$

for the prolate system, where f_s^* is the value of f_s predicted by the basal solution at the point of changeover. The reader should note that higher order derivatives are allowed to be discontinuous at the point of changeover.

Thermal matching conditions

At the point of changeover, the first law of thermodynamics requires that temperature and heat flux be continuous. Equating the heat flux predictions in the basal and tip regions at the point of changeover, we have

$$\frac{dT}{dZ^*}(\text{changeover}) = \frac{R\rho_s[f_s^* L + \mathscr{C}_s(T_\infty - T_I)]L^*}{f_s^* k_s + (1-f_s^*)k_l}. \quad (46)$$

The fact that the temperature distributions predicted by the basal and tip region solution schemes are geometrically dissimilar in shape makes compliance with the requirement of temperature continuity difficult. As an approximate criterion, the temperature predicted by the basal solution will be equated to the dendrite tip temperature,

$$T(\text{changeover}) = T_s(\eta_{tip}) = T_s(\eta_{tip}) = T_I. \quad (47)$$

The maximum error associated with this simplified criterion is 0.01 K.

Overall method of solution

A block diagram of the solution scheme is shown in Fig. 5. The method consists of two serial parts. The first part is to determine the basal temperature gradient and the axial position of changeover Z^*_{change}, using a one-point iteration scheme. These parameters are then used as boundary conditions to calculate the composite temperature and concentration fields in the second part of the procedure.

The calculation is started by guessing values for the two unknown variables. The basal region equations are then integrated from $Z^* = 0$ (basal plane) to the assumed Z^*_{change}. The resulting values of f_s and df_s/dZ^* at $Z^* = Z^*_{change}$ are used in equations (42)–(45) to obtain a and δ. The dendrite tip configuration η_{tip} is calculated from equation (31) and the tip concentration and temperature are calculated from equation (20). The degree of satisfaction of the matching criteria is determined by comparing the left and right hand sides of equations (46) and (47). If the criteria are not satisfied to acceptable accuracy, a revised guess of the basal temperature gradient and changeover position is made and the procedure is repeated. When acceptable accuracy has been obtained, the basal region and tip region equations are integrated a final time to obtain the final result.

The reader should note that the temperature, concentration and dendrite shape profiles do not depend upon the rate of freezing when described in the Z^* coordinate system. The spheroidal characteristic dimension, a is proportional to dendrite spacing (see Appendix) which is in turn proportional to R^{-1}. When the characteristic dimension, a, is substituted into equations (38)–(41) to obtain the Peclet numbers, the rate of freezing dependence is cancelled.

OVERALL RESULTS AND DISCUSSION

The overall temperature, concentration and dendrite shape results are presented in Figs. 6–9. Two independent boundary conditions are needed to specify each freezing condition: the free-field temperature and the free-field concentration. An equivalent way of expressing the temperature boundary condition is by the free-field superheat which is defined by

$$\Delta T = T_\infty - T_I(C_\infty) \quad (48)$$

where $T_I(C_\infty)$ represents the equilibrium freezing temperature at the free-field concentration.

The concentration in the liquid just adjacent to the dendrite tip, shown in Fig. 6, increases sharply with ΔT. Larger values of superheat increase the liquid phase temperature gradient, which from equation (31) is a stabilizing influence. The tips are therefore more blunt at marginal stability producing higher values of tip concentration. Tip temperature decreases with increasing tip concentration due to the assumption of thermodynamic equilibrium, in a manner similar to that shown in Fig. 4. As ΔT approaches zero, the interface concentration approaches the free-field value and the interface temperature approaches the equilibrium freezing temperature.

As material moves through the solidification zone, it undergoes three distinct energy interactions. The

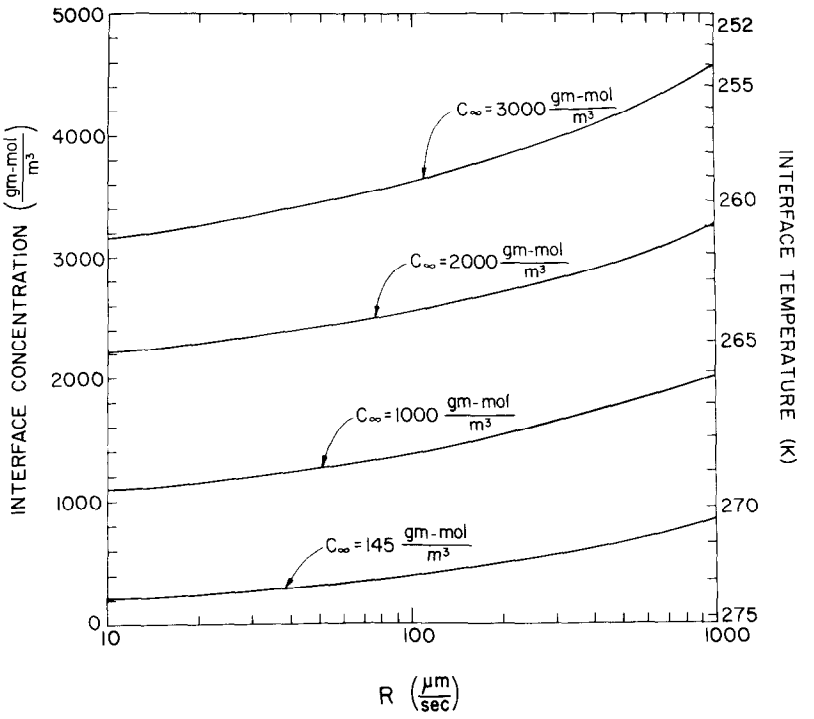

FIG. 4. Interface concentration and temperature as a function of the rate of freezing and the free-field concentrations. The dendrite frontal radius is constant at 100 μm. Note that both temperature and concentration are read from the same plot, the former from the right-hand ordinate and the latter from the left-hand ordinate.

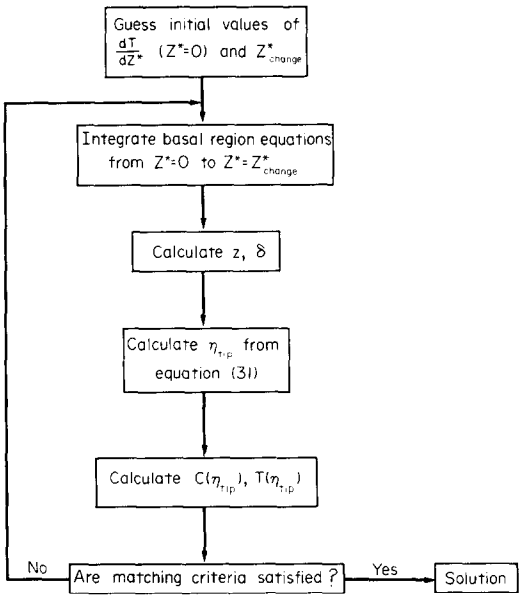

FIG. 5. Block diagram of solution technique.

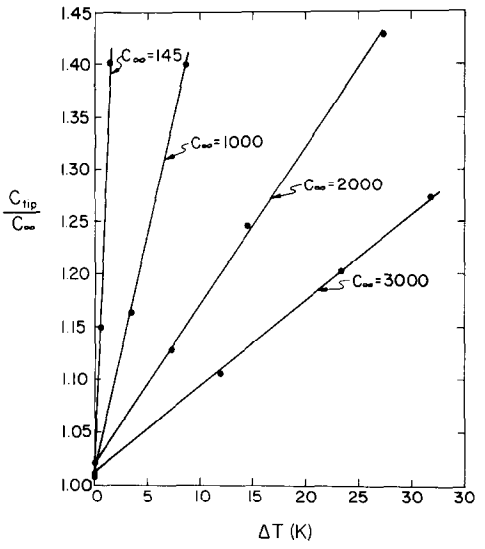

FIG. 6. Dendrite tip concentration as a function of free-field concentration and superheat.

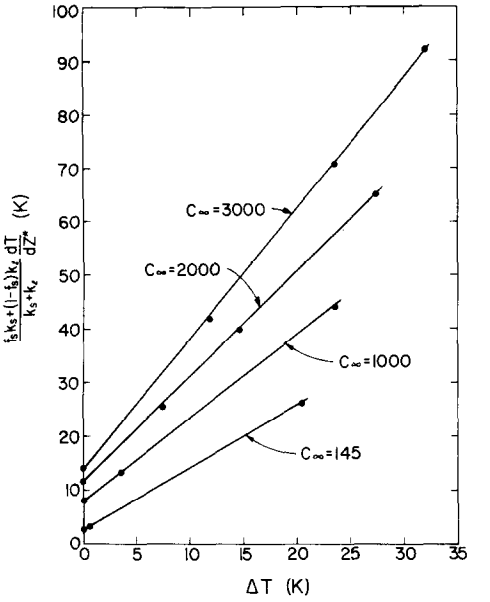

FIG. 7. Sensible heat flux at the basal plane as a function of free-field concentration and superheat.

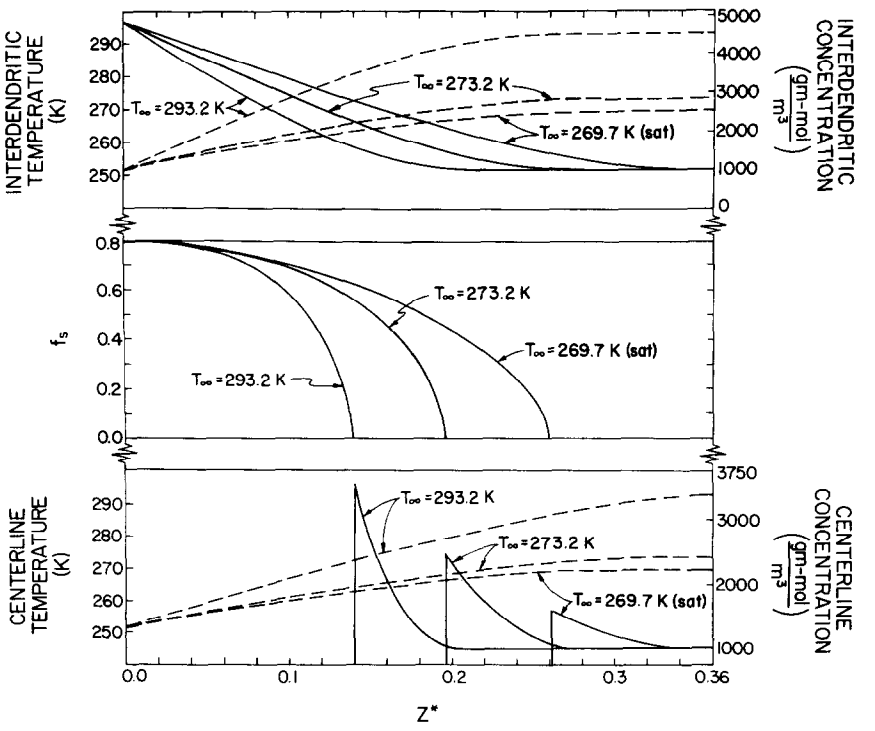

FIG. 8. Interdendritic and centerline temperature and concentration profiles and dendrite shape profiles for C_∞ = 1000 g-mol/m^3. The dashed lines represent the temperature profiles and correspond to the left-hand ordinate.

dominant interaction is the release of the latent heat of fusion, which is constant at a given free-field concentration [1, 4]. The other two energy interactions are *sensible* energy changes resulting from cooling the liquid to the freezing temperature and cooling the solid to the eutectic temperature. All of these energy interactions contribute to the required basal heat flux.

Since the release of the latent heat of fusion is not affected by ΔT, the required basal heat flux *in excess* of the latent heat flux contribution is plotted in Fig. 7. Of the two *sensible* heat interactions, the change of temperature of the liquid is the dominant factor since the thermal capacity of the liquid is twice that of the solid. The basal heat flux due to the change of temperature of the liquid is proportional to the free-field temperature, which produces the linear relationship shown in Fig. 7.

The temperature and concentration profiles along the midline between two adjacent dendrites (the interdendritic space) are shown in Figs. 8 and 9 for C_∞ = 1000 and 2000 mol/m^3 respectively. The temperature increases almost linearly from the basal plane to the point of changeover between the basal and tip regions where it approaches the free-field temperature asymptotically. Because of the assumed coupling between temperature and concentration in the basal region, the concentration *decreases* linearly and approaches C_∞ in a manner similar to the temperature.

The concentration and temperature profiles along a dendrite axis are shown in Figs. 8 and 9. The temperature profiles are identical to those on the interdendritic axis in the basal region since the temperature field was assumed to have no lateral variation in that region. However, the temperature gradient along the dendrite axis is allowed to be discontinuous at the dendrite surface by virtue of equations (29) and (30). The magnitude of this discontinuity is small enough to be quantitatively unnoticeable in Figs. 8 and 9. The concentration of solute is zero everywhere in the solid and exhibits steep profiles in the liquid just adjacent to the dendrite tips.

SUMMARY AND CONCLUSIONS

Equations describing the energy and mass transport near the tips of steadily advancing dendrites have been derived. Transformation to the oblate–prolate spheroidal coordinate system yielded 1-dim. equations which were solved analytically. Because of the $1/R$ variation of the dendrite spacing, interface speed was eliminated as an independent variable.

The solution of the 1-dim. equations show that dendrites are shorter and more blunt for both higher free-field superheat and higher free-field concentration. The required basal heat flux and dendrite tip concentration also increase sharply with increasing free-field superheat. The steep concentration profiles near the dendrite tip are made less severe by increasing tip pointedness or decreasing dendrite diameter.

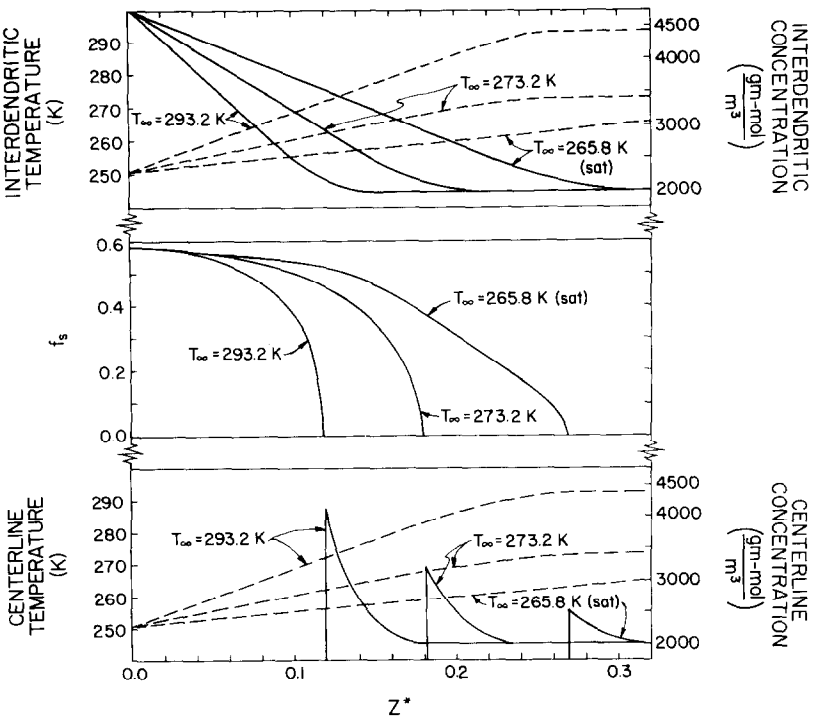

FIG. 9. Interdendritic and centerline temperature and concentration profiles and dendrite shape profiles for C_∞ = 2000 g-mol/m^3. The dashed lines represent the temperature profiles and correspond to the left-hand ordinate.

Acknowledgements—Support of this work was provided by the Whittaker Health Sciences Fund at the Massachusetts Institute of Technology. The authors also gratefully acknowledge the assistance of Ms. P. Stameris.

REFERENCES

1. M. G. O'Callaghan, E. G. Cravalho and C. E. Huggins, An analysis of heat and mass transport during solidification of an aqueous binary solution — I. Basal plane region, *Int. J. Heat Mass Transfer* **25**, 553–561 (1982).
2. G. P. Ivantsov, *Doklad. Akad. Nauk. SSSR* **58**, 567 (1947); translation "Growth of Crystals," Consultants Bureau, New York (1958).
3. W. W. Mullins and R. F. Sekerka, Stability of a planar interface during solidification of a dilute binary alloy, *J. appl. Phys.* **35**, 126–131 (1963).
4. M. G. O'Callaghan, An analysis of the heat and mass transport during the freezing of biomaterials, Ph.D. Thesis, Department of Mechanical Engineering, Massachusetts Institute of Technology, Cambridge, Mass., (October 1978.)
5. P. K. Rohatgi and C. M. Adams, Dendritic solidification of aluminum–copper alloys, *Trans. metall. Soc. A.I.M.E.* **239**, 1737–1746 (1967).
6. M. M. Yovanovich, *Advanced Heat Conduction*. Prepublication copy University of Waterloo, Waterloo, Ontario (1969).

APPENDIX

Dendrite spacing

The most recent work on dendrite spacing in aqueous systems is by Rohatgi and Adams [5]. They derived the following relationship between dendrite spacing and solidification parameters

$$L_D = (A_1 + A_2 C_\infty)\sqrt{t_f} \tag{A1}$$

where A_1 and A_2 are constants, and the characteristic freezing time t_f is defined by [4]

$$t_f = 0.25L^*/12. \tag{A2}$$

From available data, A_1 and A_2 are found to be

$$A_1 = 6.41 \times 10^{-7}\text{m-s}^{-1/2}$$

and

$$A_2 = 1.09 \times 10^{-9}\ \text{m}^4\text{-s}^{-1/2}\text{-g-mol}^{-1}.$$

ANALYSE DU TRANSFERT DE CHALEUR ET DE SOLUTE PENDANT LA SOLIDIFICATION D'UNE SOLUTION AQUEUSE BINAIRE—II. REGION DES SOMMETS DES DENDRITES

Résumé—On développe l'analyse du transfert d'énergie et de masse près des sommets de dendrites qui avancent en permanence. Des équations de transport ont été obtenues puis résolues en utilisant la méthode de changement de variable pour obtenir un système à une dimension. Des critères géométriques et thermodynamiques sont employés pour faire en sorte que les champs dans la région du sommet soient compatibles avec ceux obtenus précédemment dans la région du plan de base.

Les résultats globaux montrent que plus le champ de température est élevé, plus les dendrites sont courts et émoussés. De façon semblable, l'accroissement du champ libre de concentration avec une surchauffe constante réduite notablement la longueur des dendrites. Celle-ci est trouvée être aussi inversement proportionnelle à la vitesse de solidification.

EINE ANALYSE DES WÄRME- UND STOFFTRANSPORTS BEIM ERSTARREN EINER WÄSSRIGEN BINÄREN LÖSUNG—II. BEREICH DER DENDRITENSPITZE

Zusammenfassung—Es wurde eine Analyse des Energie- und Stofftransports in der Nähe der Spitzen von stetig wachsenden Dendriten entwickelt. Die Transportgleichungen wurden aufgestellt und durch Variablentransformation in ein eindimensionales System gelöst. Geometrische und thermodynamische Anspassungskriterien wurden eingeführt, um sicherzustellen, daß die Felder der Transportgrößen in der Spitzenregion mit denen verträglich sind, die schon früher für den Basisflächen-Bereich ermittelt wurden. Die Gesamtergebnisse zeigen, daß die Dendritenform um so kürzer und stumpfer wird, je höher die Temperatur in der Lösung ist. Ähnlich reduziert eine zunehmende Konzentration in der Lösung bei konstanter Überhitzung die Dendritenlänge drastisch. Es zeigte sich, daß die Dendritenlänge umgekehrt proportional der Gefriergeschwindigkeit ist.

АНАЛИЗ ПЕРЕНОСА ТЕПЛА И МАССЫ РАСТВОРЕННОГО ВЕЩЕСТВА ПРИ ЗАТВЕРДЕВАНИИ ВОДНОГО БИНАРНОГО РАСТВОРА — II. ОБЛАСТЬ ДЕНДРИТНЫХ ВЕРШИН

Аннотация — Проведен анализ переноса энергии и массы у вершин непрерывно растущих дендритов. Выведены уравнения переноса, которые решены методом преобразования переменных для одномерного случая. Для сопоставления результатов по переносу, полученных в области у вершин и базисной плоскости использовались геометрические и термодинамические критерии сращивания. Показано, что чем выше температура раствора, тем более короткими и пологими являются дендриты. Аналогично, при большей концентрации раствора и постоянном его перегреве длина дендритов значительно меньше. Найдено также, что длина дендритов обратно пропорциональна скорости затвердевания.